NUMERICAL SOLUTION OF AXISYMMETRIC JET-PLUME COUPLED WITH EXTERNAL FREESTREAM

Erdal YILMAZ[1] and Mehmet Şerif KAVSAOĞLU[2]
Aeronautical Engineering Department
Middle East Technical University
Ankara, TURKEY

Several methods for predicting exhaust plume boundaries with a surrounding external flow currently exists [1]. There are some experimental studies that have been performed to predict plume behavior at different jet exit pressure ratios [2,3]. When the exit pressure ratio increases then some numerical problems arise due to the solution techniques. In addition mesh adaptation is needed because the shock and plume boundary is a thin layer. Therefore to resolve such regions more accurately solution adaptive mesh generation is required. Present method solves axisymmetric Euler equations by using finite volume technique on unstructured triangular meshes. Solution adaptation has been employed considering Mach gradients. Prediction of plume boundary fits very well with the experiment.

Introduction

Exhaust plume boundary prediction has many applications in aerospace industry. In spacecrafts and ballistic missiles the extent of the plume is an important factor, since it may effect downlink communication. One another important consideration is that infrared radiation of plume increases at high altitudes just due to the expansion of the plume. Because pressure decreases in the order of a hundreds or sometimes a thousands. Also, an understanding of the interaction between exhaust plume and various vehicle components such as control fins, necessitates exhaust plume prediction for aircrafts, missiles and spacecrafts. An exhaust plume expansion into a supersonic external freestream further complicates the flow field. Because plume boundary behaves like a curved rigid body so that it causes shock wave mostly a curved shock not oblique. Therefore it's strength is not low. Very large gradients exists around these regions.

A review of available techniques revealed that there are very few methods for the prediction of plume characteristics especially by CFD [1,8]. In the present investigation a practical and accurate solution technique [4] is applied to such problems.

Governing Flow Equations

The flow inside a duct and the flow around a body of revolution possess axial symmetry at zero angle of attack because of the circular crossection of the body. The coordinates are r ,θ , z where r is the radius to the projection on the xy plane, z is the distance above the xy plane and θ is the angle between the radius r and x axis.

For an axisymmetric flow both the velocity component v_θ and derivative with respect to θ are set to zero. The resulting axisymmetric equation in cylindrical coordinate is

$$\frac{\partial U}{\partial t} + \frac{\partial F}{\partial z} + \frac{1}{r}\frac{\partial (rG)}{\partial r} - \frac{G^*}{r} = 0 \qquad (1)$$

where U is called solution vector and represents the conserved quantities. F and G are the Cartesian components of the flux vector of these quantities. More explicitly , they are defined as

$$U = \begin{pmatrix} \rho \\ \rho u \\ \rho v \\ \rho E \end{pmatrix} \quad F = \begin{pmatrix} \rho u \\ \rho u^2 + p \\ \rho uv \\ \rho uH \end{pmatrix}$$

$$G = \begin{pmatrix} \rho v \\ \rho uv \\ \rho v^2 + p \\ \rho vH \end{pmatrix} \quad G^* = \begin{pmatrix} 0 \\ 0 \\ p \\ 0 \end{pmatrix} \qquad (2)$$

[1] Ph.D. Student.
[2] Associate Professor, Senior Member AIAA.

and

$$E = \frac{p}{(\gamma - 1)\rho} + \frac{u^2 + v^2}{2} \quad , \quad H = E + \frac{p}{\rho} \qquad (3)$$

If the third term of equation(1) in space is expanded then following form with a source term is obtained.

$$\frac{\partial U}{\partial t} + \frac{\partial F}{\partial z} + \frac{\partial G}{\partial r} + H^* = 0 \qquad (4)$$

where

$$H^* = \frac{1}{r}\left(\rho v, \rho uv, \rho v^2, \rho vH\right)^T \qquad (5)$$

Equation (4) is equivalent to the following 2D equation in Cartesian coordinates.

$$\frac{\partial U}{\partial t} + \frac{\partial F}{\partial x} + \frac{\partial G}{\partial y} + \alpha H^* = 0 \qquad (6)$$

here α is "0" for two dimensional problems and "1" for axisymmetric problems. In this form , the above equations apply to a particular point in space. If one wishes to apply them to entire region of the flow field, one may integrate them over the whole control volume. The differential formulation is converted to the integral form by application of the Gauss's theorem in the plane, then following equation is obtained.

$$\frac{\partial}{\partial t}\int_{\Omega} U d\Omega + \oint_{S}\left(F dy - G dx\right) + \alpha \int_{\Omega} H^* d\Omega = 0 \qquad (7)$$

This is the equation to be solved throughout this study.

Numerical Solution Technique

The equation (7) is discretized in space by using finite volume formulation. Artificial dissipation terms are employed to damp oscillation due to the numerical solution method. Multi-stage time discretization is used in advancing time. First, the whole domain is subdivided into a large number of small control volumes. When the integral equation is applied to each control volume, it results in a set of ordinary differential equations which can be solved by marching in time [4,7].

When the integral form of the Euler equations are applied to a finite control volume Ω_K , one obtains the following coupled ordinary differential equations

$$\frac{\partial}{\partial t}\left(U_K \Omega_K\right) + \sum_{i}^{Nedge}\left(F_i \Delta y_i - G_i \Delta x_i\right) + \alpha\left(H_K \Omega_K\right) = 0 \qquad (8)$$

for each control volume around K, where Ω_K is the control volume associated with the node K , U_K is the solution vector at node K , F_i and G_i are the Cartesian components of the flux vector on face i of the control volume, Nedge is the total number of edges which surround the control volume, $\Delta x_i, \Delta y_i$ are the incremental distance of x and y along face i , see figure-1 . H_K is the additional terms at node K due to the axisymmetry, hereafter H is used instead of H*. The fluxes F_i and G_i are functions of flow variables at neighboring points, and thus the system of equation is coupled in space. Here the control volume is performed in a similar way of the evaluation of the fluxes. Note that for 2D cases a discrete control volume is defined as the area around a point enclosed by edges of meshes as given in figure-1.

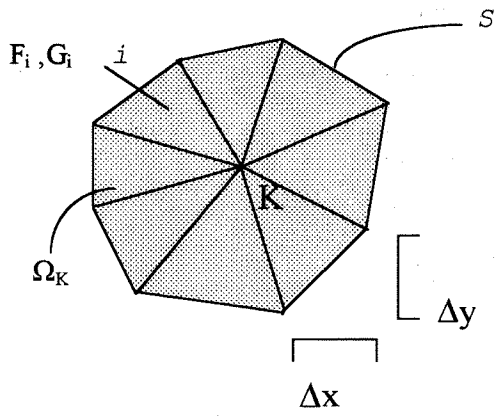

FIGURE 1 - A finite control volume at node K

The sum of the flux terms refer to all external sides of the control volume Ω_K . For the whole domain , control volumes associated with the nodes will overlap. This , however doesn't produce any difficulty since each edge produce a positive flux contribution to one neighbouring control volume, and a negative flux

contribution to other neighbouring control volume and no contribution when it is internal to a control volume.

Since the nodal scheme involves the evaluation of the fluxes across the edges of the triangular cells, the most basic element of the mesh is seen to be the side, rather than the triangular cell itself. Therefore the data structure of the mesh, called as mesh connectivity, is based on the sides

Artificial Dissipation

In the above form, the discretized equations contain only first differences between flow variables thus are non-dissipative. This means that background errors, such as discretization or round-off errors , are not damped and oscillations may be present in the steady state solution. Also oscillations may be produced in regions of large pressure gradients such as near shocks, and will persist due to the non-dissipative nature of these scheme. In order to eliminate these oscillations, artificial dissipation terms are added to the equation (8).

The approach of Jameson et al [6,7] is adopted to construct the dissipation function. This consists of a blend of second and forth differences of the flow variables U .

Time - Stepping

The system of ordinary differential equations (8) represents an initial value problem which must be solved in order to obtain the steady-state solution , that is until the time derivatives all vanish. Since the cell area Ω_K for each cell K is fixed, then the equation (8) may be rewritten as

$$\frac{dU_K}{dt} + R(U_K) = 0 \qquad (9)$$

where R is the residual. The integration in time to a steady state solution is performed using a multi-stage scheme. Since the time accuracy to a steady state solution is not important for a steady state solution, such schemes are selected only for their properties of stability and damping

A slightly different class of schemes can be constructed by separating, within R_K itself, the evaluation of the convective and dissipative operators. A saving in computational effort and altering the properties of the scheme may be achieved by omitting the re-evaluation of the dissipative operator at each stage. This is known to modify stability region of the scheme, but the steady-state accuracy and convergence characteristics appear to be preserved. Such schemes are called hybrid multi-stage time stepping schemes. For a q-stage scheme, equation (9) takes the following

$$\begin{aligned} U_K^0 &= U_K^n \\ U_K^1 &= U_K^0 - \alpha_1 \Delta t_K R_K^0 \\ &\cdot \\ U_K^q &= U_K^0 - \alpha_q \Delta t_K R_K^{q-1} \\ U_K^{n+1} &= U_K^q \end{aligned} \qquad (10)$$

This is a fully explicit scheme where Δt is discrete time step and $\alpha_1 \ldots \alpha_q$ are coefficients particular to the time stepping schemes. n is the known time step. For a three-stage scheme the coefficients are 0.8, 0.8 and 1. , for a four-stage scheme they are 0.25, 1./3., 0.5 and 1.0

Convergence Acceleration

An efficient Euler solver must be rapidly convergent. The generally known methods for the convergence acceleration are local time stepping, residual averaging, adaptive remeshing, entalphy dumping and multigrid algorithms. Local time stepping advances the equation in time by taking the maximum permissible time step at each cell in the mesh. Residual averaging seeks to relieve the Courant-Fredrich-Lewy (CFL) limitation on the time step by increasing stability. Enthalpy damping uses a slight modification of the Euler equation to provide additional damping in time. Multigrid algorithms perform time steps on coarser meshes to accelerate the solution on a fine mesh. Adaptive remeshing algorithms increases the density of the mesh in high gradient region while decreasing the mesh density in low gradient region at subsequent time steps. In the present study the first three methods are employed in the solution algorithm.

Initial and Boundary Conditions

Freestream values are used as initial conditions in the entire domain of interest. In the grid file boundary edges are marked with different indexes corresponding to different boundary conditions. Following numbers are

used together with boundary edges for different boundary conditions.

1	inviscid wall,	5	far field (outflow)
2	isothermal wall,	-5	far field (inflow)
3	adiabatic wall,	-6	jet outflow (or inflow)
4	symmetry condition		

For inviscid flow , the required boundary condition at surfaces of object is flow tangency or no flow normal to the boundary. This is easily implemented by setting the convective fluxes to zero along all mesh edges which coincide with the surface of object.

In the present calculations isothermal and adiabatic wall conditions are not used. Along the symmetry line normal velocities are set to zero and gradients of the axial velocity are extrapolated from the interior points connected to the boundary edge. At far field vortex corrections are used if the object generates lift and flow is subsonic. However this is not the case in axisymmetric problems. If the flow is supersonic or axisymmetric then nothing is done except the extrapolation from interior points. This is accomplished by adding half of the unknowns of the interior points to the corresponding end-points of the boundary edge using the information of grid connectivity at boundary edges

Adaptive Mesh Refinement

The mesh generation is the division of the solution domain into discrete inter-connected points called grid points. The grid points in the inner domain are usually positioned so that they are concentrated in regions where it is expected that there will be large gradients (such as near shock waves) and are relatively sparse in regions where the solution is expected to vary slowly. This leads to the adaptive grid generation procedure in which the grid generator and flow solver interacts. By using the solution and corresponding grid a sensor value is obtained through which new spacing of the previous grid is found [5]. After that grid generator is activated to find new grid using new grid spacing values.

For Euler equations, some of the main flow features of the solution can be shock waves, stagnation points and vortices and any indicator should accurately identify these flow characteristics. The method which has been chosen to identify these important flowfield features is a measure of the gradient of some dependent variable Q . Several different physical criteria have been proposed for Q ,in this study following combination is assumed.

$$Q = a.\rho + b.p + c.u + d.v + e.M \qquad (11)$$

where a, b, c, d and e are weighting factors for corresponding flow parameters. The criteria which have been tested are local Much number, density, pressure and velocities. The criteria are written as the gradient of these quantities in the stream direction. For Euler equations following are used.

$$|u.\nabla Q| \text{ and } |\nabla Q| \qquad (12)$$

where u is the velocity and Q is Mach number or density or pressure or velocity.

Discussion of Results

In this study very high pressure ratio jet plume coupled with a supersonic external stream is examined. Figure-2 gives the typical flow structure of such problems. Since the pressure ratio is very high sometimes manipulations are needed to start a smooth solution. Therefore pressure at the exit is steadily increased to the final desired pressure. And then solution is proceeded until the convergence is achieved. A coarse mesh is generated as an initial mesh. It is given in Figure-3.

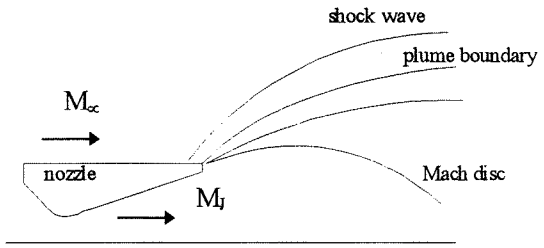

FIGURE 2 - Typical Underexpanded Plume

Pressure ratios at the exit are increased steadily by powers of 2 starting from 0 to 10 . At each step a hundred iterations is performed as an initial condition to the next step. After the last step pressure ratio is increased to 1500. With this ratio further five hundreds iterations are performed so that required gradients of flow parameters are developed. Then the solution and corresponding mesh are feed to the mesh adaptation procedure.

In this part gradient of Mach number is used as a mesh refinement criteria. This is most suitable parameter for plume external freestream flow problems. Because through the shock wave and plume boundary Mach number is the most dominant parameter to be considered. In the mesh adaptation, the density of mesh is increased in high gradient regions while it is decreased in low gradient regions [5]. It is also possible just to increase the mesh density. But to avoid

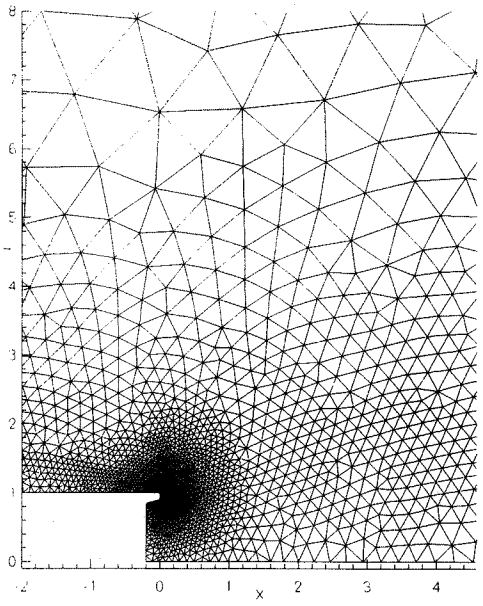

FIGURE 3 - Initial Mesh

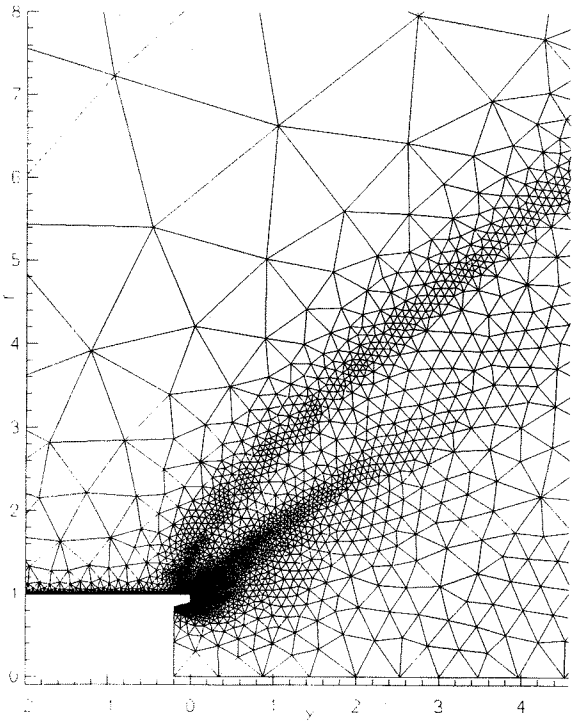

FIGURE 4 - Adapted Mesh

unnecessary fine meshes, meshes are removed from the low gradient parts of the flow. After the determination of mesh spacing values mesh generation procedure is employed using new spacing values. With this new mesh the above procedure is repeated three times. In the last step of the final stage, number of iteration is increased to three thousands. Figure-4 and 5 gives the adapted meshes in detail.

As it is obvious from the meshes, there are basically two high gradient regions; one is the shock wave of the external freestream due to the plume shape, and the other is plume boundary itself. Therefore meshes are made very dense in these regions. The minimum size of the mesh is determined by user's intention. Since the flow is supersonic and we are interested in the plume boundary the solution domain is kept as much as small.

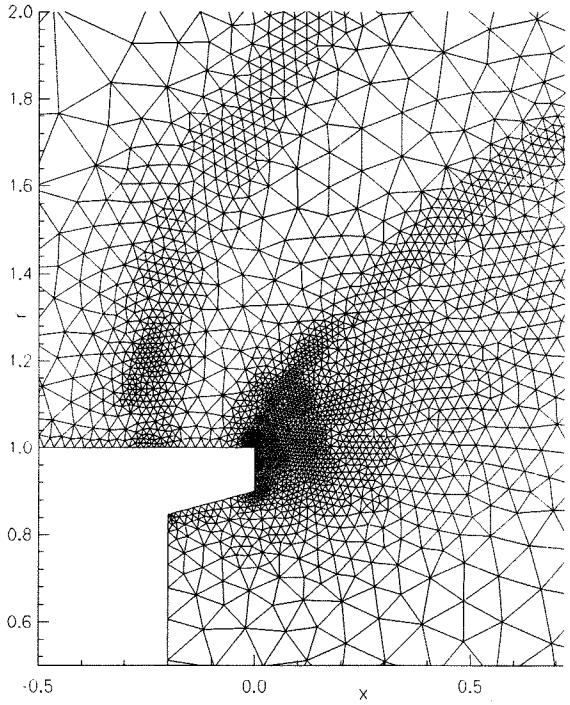

FIGURE 5 - Adapted Mesh in Detail

Specific heat ratio is taken as 1.4 and jet exit angle is 15 degrees. Freestream Mach number for the first case is taken as 4. Mach contours are shown in figure-6. The shock wave due to plume and plume boundary is obvious. The shock wave is not oblique around the nozzle exit but actually it is a bow shock therefore stronger than oblique shock wave. If some external components are to be used around the nozzle location of this shock and strength of it must be taken into account. Between the shock wave and plume boundary Mach number first decreases and then increases

until to the plume boundary. After that it suddenly increases to almost ten up to the Mach disc.

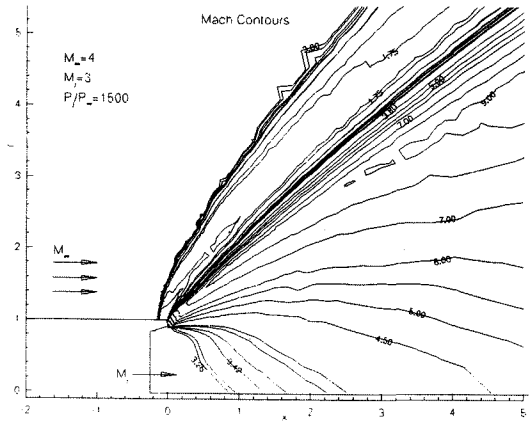

FIGURE 6 - Mach Contours for $M_\infty = 4$

Streamlines, which shows flow direction clearly, are given in Figure-7. Jet plume behaves like a solid boundary. Just after the shock wave flow deflects parallel to the plume boundary and then it maintains same direction. Flow overexpands to the freestream after leaving the exit plane.

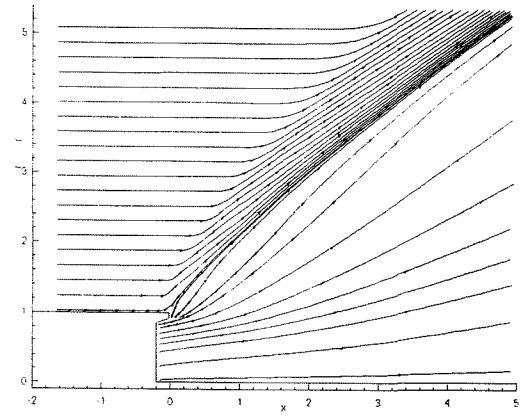

FIGURE 7 - Streamlines for $M_\infty = 4$

The residual history plot for the last adaptation stage is given in Figure-8. Residual is taken as the maximum error of flow variables, in this case density, scaled by local time steps between two iteration steps. Steady pressure increase at each 100 iteration causes an increase in the residual. When the pressure is increased to 1500 at the jet exit, then it jumps suddenly from order two to five. And then it starts to converge. It seems that a thousand iteration is enough for convergence to order zero. After that it doesn't converge furthermore.

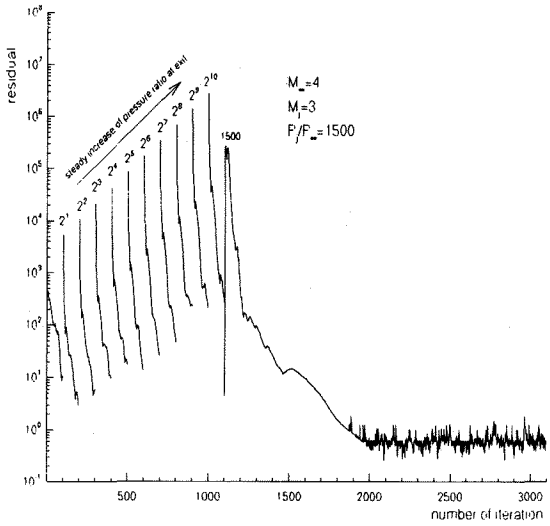

FIGURE 8 - Residual History for $M_\infty = 4$

Comparison of the plume boundary is done in Figure-9 and 10. Computation almost fits with the experiment [2]. There are very minor errors only. There may be some errors in the extraction of the experimental and computational data. It seems that plume shape changes almost linearly for a very short distance. And then starts to curve down as it goes downstream. When the external freestream is five then computation underpredicts but it is finite.

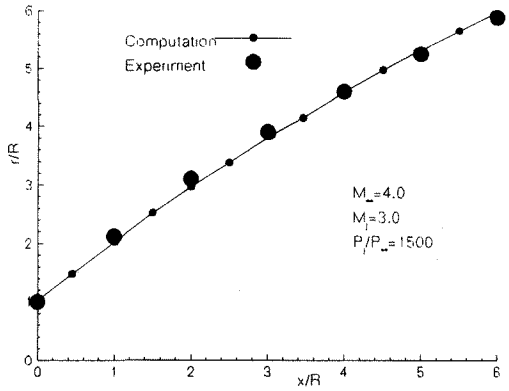

FIGURE 9 - Comparison of Plume Shape, $M_\infty = 4$

Finally some case studies are done for different exit pressure ratios which are 1 and 10. Freestream and jet exit Mach number are taken as 3. Initial coarse mesh is used as the computational mesh. Figure 11 to 12 give

the Mach contours for these cases. The change of plume shape and shock structure is clearly shown. Expansion of the Mach numbers from exit to the Mach disc is indicated. How the thickness of the shear layer changes is observed.

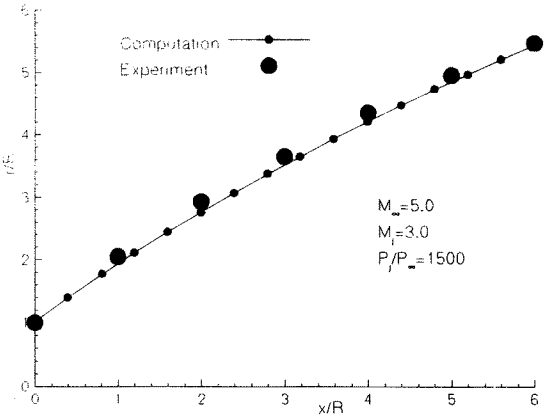

FIGURE 10 - Comparison of Plume Shape, $M_\infty = 5$

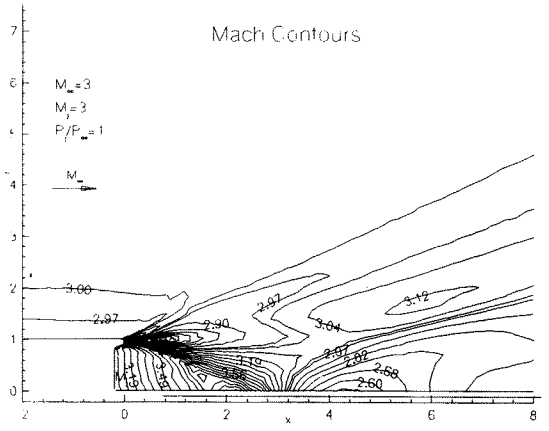

FIGURE 11 - Mach Contours, $P_j / P_\infty = 1$

Conclusions

An axisymmetric Euler solution technique was used to predict the jet plume and freestream interaction. Triangular meshes was used with suitable adaptation techniques. It was observed that not only the plume boundary was predicted but also the domain was solved correctly. And the information that can be extracted is more than one which calculates plume boundary only. Accuracy depends on the initial mesh and adapted meshes strongly. Therefore one should carefully attack to the problem. If the upstream external shape of the nozzle is not smooth then flow structure can be predicted by this technique. However in such cases boundary layer would be dominant therefore Navier-Stokes solution is required. The cost of this solution is found to be low for a computational technique.

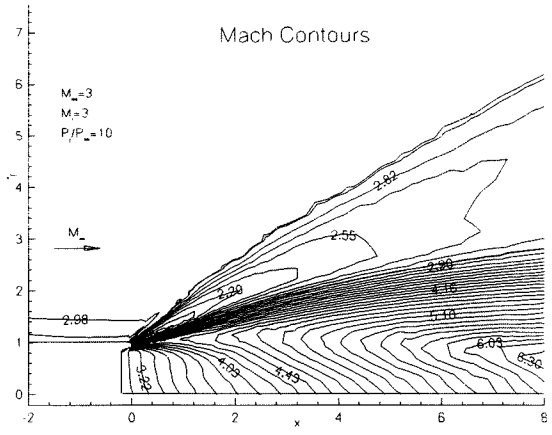

FIGURE 12 - Mach Contours, $P_j / P_\infty = 10$

References

[1] Nash et al, "Predicting Exhaust Plume Boundaries with Supersonic External Flow.", J. Spacecraft and Rockets, pp 773-777, Sept-1994.

[2] Henson, J.R., and Robertson, J.E., "Methods For Aproximating Inviscid Jet Boundaries For Highly Underexpanded Supersonic Nozzles." AEDC-TN-67-2, Arnold Engineering Development Center, Tullahoma, Tn, May. 1962

[3] Latvala, E.K, and Anderson, T.P., " Experimental Determination of Jet Speading From Supersonic Nozzles at High Altitudes." , AEDC-TN-58-98, Arnold Engineering Development Center, Tullahoma, Tn, Nov. 1958.

[4] Yılmaz, E. "Two Dimensional And Axisymmetric Euler Solution on Unstructured Grids", M.S. Thesis, Dec. 1994, Middle East Technical University, Ankara, TÜRKİYE.

[5] Yılmaz, E. and Dilaver, S. ," Implementation of Grid Adaptivity to a Two Dimensional and Axisymmetric Euler Solver.", TUBITAK-SAGE, EY-No: 23107, Jan. 1995.

[6] Jameson et al, "Numerical Solution of Euler Equations by Finite Volume Methods Using Runge Kutta Time Stepping Schemes", AIAA Paper 81-1259.

[7] Mavripilis, D., " Solution of Two Dimensional Euler Equations on Unstructured Triangular Meshes", Ph.D. Thesis. Princeton University, USA,June 1987.

[8] Weinacht, P., and Sahu, J., "Navier Stokes Predictions of Missile Aerodynamics", AGARD R-808, June 1994.